Osteoblast/osteocyte-derived interleukin-11 regulates osteogenesis and systemic adipogenesis

Bingzi Dong
Tokushima University Graduate School of Medical Sciences
Masahiro Hiasa
Tokushima University Graduate School of Medical Sciences
Itsuro Endo
University of Tokushima
Yukiyo Ohnishi
Tokushima University Graduate School of Medical Sciences
Takeshi Kondo
Tokushima University Graduate School of Medical Sciences
Yuichi Takashi
Tokushima University
Maria Tsoumpra
Tokushima University
Risa Kainuma
Tokushima University
Shun Sawatsubashi
Tokushima University
Hiroshi Kiyonari
RIKEN Center for Biosystems Dynamics Research https://orcid.org/0000-0002-1509-8747
Go Shioi
RIKEN Center for Biosystems Dynamics
Hiroshi Sakaue
Department of Nutrition, Tokushima University https://orcid.org/0000-0002-2468-2363
Tomoki Nakashima
Tokyo Medical and Dental University
shigeaki kato
Iryo Sosei University https://orcid.org/0000-0002-5564-1695
Masahiro Abe
University of Tokushima
Seiji Fukumoto
University of Tokushima https://orcid.org/0000-0003-3610-3469
Toshio Matsumoto (toshio.matsumoto@tokushima-u.ac.jp)

Tokushima University https://orcid.org/0000-0002-0618-0941

Article

Keywords: Fat metabolism, (IL)-11, mechanical loading

Posted Date: September 30th, 2021

DOI: https://doi.org/10.21203/rs.3.rs-888146/v1

Version of Record: A version of this preprint was published at Nature Communications on November 23rd, 2022. See the published version at https://doi.org/10.1038/s41467-022-34869-3.

Abstract

Exercise offers mechanical loading to the bone, while it stimulates energy expenditure in the adipose tissue. Thus, bone may secrete a factor to communicate with adipose tissue in response to mechanical loading. Interleukin (IL)-11 is expressed in the bone, upregulated by mechanical loading, enhances osteogenesis and suppresses adipogenesis. Systemic IL-11 deletion (IL-11$^{-/-}$) exhibited reduced bone mass, suppressed bone formation response to mechanical loading, enhanced expression of Wnt inhibitors, and suppressed Wnt signaling. Enhancement of bone resorption under mechanical unloading was unaffected. Unexpectedly, IL-11$^{-/-}$ mice showed increased systemic adiposity and glucose intolerance. Osteoblast/osteocyte-specific IL-11 deletion in osteocalcin-Cre;IL-11$^{fl/fl}$ mice showed reduced serum IL-11, blunted bone formation under mechanical loading, and increased systemic adiposity similar to IL-11$^{-/-}$ mice. Adipocyte-specific IL-11 deletion in adiponectin-Cre; IL-11$^{fl/fl}$ mice exhibited no abnormality. Thus, IL-11 from osteoblast/osteocyte controls both osteogenesis and systemic adiposity in response to mechanical loading. These findings may bring new therapeutic approaches to osteoporosis and metabolic syndrome.

Introduction

Exercise offers mechanical loading to maintain bone remodeling balance and muscle strength, while it stimulates energy expenditure in the adipose tissue. As these responses are simultaneously and rapidly evoked, metabolic communications among tissues appear to underlie the systemic response. Because bone is an endocrine organ controlling mineral homeostasis [1, 2] as well as energy expenditure [3], we assumed presence of an exercise sensor derived from bone to communicate with the adipose tissue for energy expenditure. We have previously found that interleukin (IL)-11 is expressed mainly in the bone and is upregulated by mechanical loading to bone [4]. Because the biological activity of IL-11 was originally reported to inhibit adipogenesis of bone marrow adipocytes *in vitro*, and designated also as adipogenesis inhibitory factor (AGIF) [5], there is a possibility that IL-11 may be the factor coupling exercise-induced changes in bone remodeling with those in adipose tissue metabolism.

IL-11 is one of interleukin members which were originally identified as cytokines secreted from helper T cells. Further studies have uncovered broader spectrum of biological actions of IL-11 including regulation of hematopoiesis [6], cancer development/progression [7], and mesenchymal cell differentiation [8]. As to its biological action on bone remodeling, a detailed dissection of IL-11 action showed that IL-11 enhanced osteoclast formation and bone resorption [9], and this activity was later shown to be mediated by stimulation of osteoblastic differentiation from mesenchymal progenitors [10]. There was also a report that IL-11 receptor α knockout (IL-11Rα$^{-/-}$) mice exhibited increased bone mass with cell-autonomous reduction in osteoclast precursor differentiation [11]. From those results, the physiological role of IL-11 for bone remodeling has been considered as an osteoclastic regulator. However, on the contrary, when IL-11 was overexpressed in transgenic mice, bone formation and bone mass were unexpectedly increased

without changes in osteoclastic bone resorption [12]. Moreover, these mice were resistant to age-related bone loss. Thus, controversy evidently remains as to the role of IL-11 on bone remodeling.

Mechanical loading to osteoblastic cells stimulates Ca^{2+} influx which activates cAMP-responsive element binding protein (CREB) signaling via extracellularly regulated kinase (ERK) in osteoblasts, and activated CREB enhances ΔFosB expression [13], suggesting that ΔFosB is a sensing regulator of mechanical loading in gene regulatory cascade. As mechanical loading induces orchestral response in bone remodeling, a number of genes are conceivably responsive to ΔFosB expression. We have already reported that ΔFosB/JunD heterodimer binds to AP-1 sites on *IL-11* gene promoter and that indeed upregulates *IL-11* gene transcription with osteoblast differentiation in response to mechanical loading [4]. Gene expression analysis further found that Wnt signaling is enhanced via suppression of Wnt inhibitors by IL-11 stimulation, suggesting that the IL-11 response to mechanical loading in bone remodeling may result in activation of Wnt signaling [4]. The cascade of the IL-11 stimulation to osteoblast differentiation is modulated by other factors. Parathyroid hormone acts as a positive hormone, while glucocorticoid and aging are negative factors [14, 15]. Those past findings look favorable in the effect of IL-11 on bone formation, but the *in vivo* role of IL-11 in regulating osteoblast differentiation and bone formation remains elusive.

To illustrate the physiological impact of IL-11 in intact animals, a series of genetically manipulated mouse lines were generated. Systemic deletion of *IL-11* gene in mice caused a reduction in Wnt signaling and in bone mass with suppressed bone formation. To our surprise, *IL-11* gene deletion also caused an increase in the systemic white adipose tissue (WAT) with glucose intolerance. Therefore, we further created osteocalcin (Ocn)-Cre;IL-$11^{fl/fl}$ mice and adiponectin (Apn)-Cre; IL-$11^{fl/fl}$ mice to examine the role of osteoblast/osteocyte-derived and adipocyte-derived IL-11 actions on the regulation of bone and adipose tissue mass. Such tissue-specific manipulation of *IL-11* gene should define the role of osteoblast/osteocyte-derived IL-11 in stimulation of osteogenesis along with regulation of systemic adiposity and energy metabolism. Thus, the present study illustrates the physiologically significant role of osteoblast/osteocyte-derived IL-11 on not only skeletal but also adipose tissue mass.

Results

Total, cortical and cancellous bone mineral density (BMD) of the vertebra and femur of IL-$11^{-/-}$ mice was reduced after weaning (Fig. 1a-1c). BMD of calvaria, a non-weight-bearing bone, in IL-$11^{-/-}$ mice was almost the same as that in WT mice (Fig. 1d), similar to that in unloading conditions [16, 17]. Vertebral histomorphometric analysis confirmed reduced bone mass in IL-$11^{-/-}$ mice with reduced bone formation and unchanged bone resorption (Fig. 1e).

Quantitative PCR of femurs revealed that expression of osteogenic genes, *Ocn*, *Runx2* and *Osterix (Osx)* was reduced in IL-$11^{-/-}$ mice, while the expression of *receptor activator of NF-κB ligand (RANKL)* and *osteoprotegerin (OPG)* as well as *RANKL/OPG* ratio was unchanged and that of osteoclastic genes,

cathepsin K (Ctsk) and *tartrate-resistant acid phosphatase (Trap)*, was not different from wild-type (WT) mice (Fig. 2a). Serum bone formation markers, osteocalcin (Ocn) and alkaline phosphatase (ALP), were reduced, whereas a bone resorption marker, TRAP, was not changed in IL-11$^{-/-}$ mice (Fig. 2b). Expression of Wnt inhibitor genes, *Sost*, *Dickkopf1 (Dkk1)* and *Dkk2*, increased in the femur of IL-11$^{-/-}$ mice (Fig. 2c), and that of Wnt target genes, *Axin2*, *Cyclin D1 (Ccnd1)* and *Ccnd4*, was reduced (Fig. 2d). We backcrossed TOPGAL mice with IL-11$^{-/-}$ mice (TOPGAL;IL-11$^{-/-}$) to detect Wnt signaling *in vivo*. TOPGAL;IL-11$^{-/-}$ mice exhibited less X-gal positive osteoblasts and osteocytes compared to TOPGAL;WT mice (Fig. 2e). Immunostaining of Wnt inhibitors, sclerostin, Dkk1 and Dkk2 was increased in IL-11$^{-/-}$ mice (Fig. 2e). Thus, the enhanced expression of Wnt inhibitors in the bone was associated with reduced Wnt signaling, which appeared to play a role at least in part in the reduction of bone formation in IL-11$^{-/-}$ mice.

In order to clarify whether the effects of IL-11 were mediated via its receptor, IL-11 receptor α (IL-11Rα), the signaling pathway of IL-11 in osteoblastic cells was examined using control and IL-11Rα knockout (KO) MC3T3-E1 cells (**Supplementary Fig. 1a-1c)**. In control MC3T3-E1 cells, IL-11 treatment enhanced phosphorylation of STAT1 and STAT3 within 15 minutes. In contrast, phosphorylation of both STAT1 and 3 was abolished in IL-11Rα KO cells (Fig. 2f). In IL-11Rα KO cells, the expression of *Rankl* and *Opg* mRNA was not different from that in control MC3T3-E1 cells. However, *Sost* mRNA was higher in IL-11Rα KO cells compared to that in control cells (Fig. 2g). These results demonstrate that IL-11 acts on osteoblastic cells via IL-11Rα to enhance STAT1,3 phosphorylation and suppress *Sost* gene expression without affecting *Rankl* or *Opg* expression.

Because mechanical loading enhanced IL-11 expression in osteoblasts [4], the role of IL-11 on unloading and reloading-induced changes in bone was examined using IL-11$^{-/-}$ mice. After tail suspension, vertebral cancellous BMD decreased in both WT and IL-11$^{-/-}$ mice (Fig. 3a). After reloading, vertebral cancellous BMD of WT mice increased to ground control level, whereas that of IL-11$^{-/-}$ mice did not reach ground control level (Fig. 3a, 3b). Expression of *Sost*, *Dkk1* and *Dkk2* genes increased by unloading and returned to the baseline by reloading in WT mice, while expression of these genes was higher at baseline and did not change by unloading or reloading in IL-11$^{-/-}$ mice (Fig. 3c). Bone histomorphometric analysis revealed that bone formation parameters were suppressed and bone resorption parameters were elevated by unloading in both WT and IL-11$^{-/-}$ mice. After reloading, although bone resorption parameters decreased and bone formation parameters increased to baseline level in WT mice, bone formation parameters did not recover fully while bone resorption parameters decreased to baseline level in IL-11$^{-/-}$ mice (Fig. 3d). Serum IL-11 in WT mice was reduced after unloading, and recovered to baseline level after reloading (Fig. 3e). Because *IL-11* expression was much higher in bone than in other tissues (**Supplementary Fig. 2**), serum IL-11 appeared to originate mostly from bone. These data demonstrate that mechanical loading enhances the production of IL-11 in the bone which suppresses the expression of Wnt inhibitors, while in IL-11$^{-/-}$ mice the production of IL-11 in the bone is not increased by mechanical loading and bone formation response to mechanical reloading is blunted.

In IL-11$^{-/-}$ mice, bone marrow adiposity increased (Fig. 4a), and adipocytic differentiation of bone marrow stromal cells (BMSC) was enhanced (Fig. 4b,4c). Addition of IL-11 suppressed adipocytic differentiation of BMSC in WT and IL-11$^{-/-}$ mice (Fig. 4b,4c). Osteoblast differentiation of BMSC from IL-11$^{-/-}$ mice was reduced (**Supplementary Fig. 3)**. Expression of osteogenic genes, *Ocn, Runx2* and *Osx*, decreased, while that of adipogenic genes, *peroxisome proliferator-activated receptor γ (Pparγ)* and *CCAAT enhancer binding protein α (Cebpα)* increased in BMSC from IL-11$^{-/-}$ mice (Fig. 4d). In addition to the increase in bone marrow adiposity in IL-11$^{-/-}$ mice, adipose tissue (AT) weight was higher in IL-11$^{-/-}$ mice under both regular diet (RD) and high fat diet (HFD) (**Supplementary Fig. 4**), and total, visceral and subcutaneous AT area was larger (Fig. 4e,4f, **Supplementary Fig. 5**). Body weight gain and size were not significantly different between WT and IL-11$^{-/-}$ mice (**Supplementary Fig. 6a,6b**), and weight of other tissues was not different between WT and IL-11$^{-/-}$ mice (**Supplementary Fig. 4**). Serum leptin and adiponectin levels were similar under RD in WT and IL-11$^{-/-}$ mice, but IL-11$^{-/-}$ mice showed higher leptin and lower adiponectin levels than WT mice under HFD (Fig. 4g). Adipocyte diameter and relative number increased in IL-11$^{-/-}$ mice (Fig. 4h, **Supplementary Fig. 7a,7b**).

Brown AT (BAT) weight and expression of BAT-specific genes, *Pparγ coactivator (Pgc)-1α* and *uncoupling protein (Ucp)-1*, were not different between WT and IL-11$^{-/-}$ mice (Fig. 5a). Expression of lipolytic enzyme genes, *hormone-sensitive lipase (Hsl)* and *adipose triglyceride lipase* (*Atgl*), in white adipose tissue (WAT) decreased in IL-11$^{-/-}$ mice, while expression of fatty acid β-oxidation enzyme, *acyl-CoA oxidase* (*Aco)*, and lipogenic enzyme, *acetyl-CoA carboxylase* (*Acc)*, was similar in both mice (Fig. 5b).

X-gal staining of tissues from TOPGAL;WT and TOPGAL;IL-11$^{-/-}$ mice indicated reduced Wnt signaling in the AT in IL-11$^{-/-}$ mice (Fig. 5c). Expression of *Dkk1* and *Dkk2* mRNA in WAT increased in IL-11$^{-/-}$ mice, and decreased by HFD in WT but not in IL-11$^{-/-}$ mice (Fig. 5d), demonstrating that Wnt signaling was suppressed in WAT of IL-11$^{-/-}$ mice via enhanced Wnt inhibitor expression. Inflammatory cytokines, *monocyte chemoattractant protein 1* (*MCP1)* and *tumor necrosis factor α* (*TNFα)*, mRNA expression in WAT was higher in IL-11$^{-/-}$ mice, and HFD enhanced expression of these cytokines in both WT and IL-11$^{-/-}$ mice (Fig. 5e). Blood glucose was higher by oral glucose tolerance test (oGTT), and area under the curve (AUC) was larger in both RD and HFD-fed IL-11$^{-/-}$ mice (Fig. 5f). Fasting level and AUC of serum insulin in oGTT as well as homeostasis model assessment of insulin resistance (HOMA-IR) were higher in IL-11$^{-/-}$ mice (Fig. 5g). These results altogether indicate that IL-11$^{-/-}$ mice develop insulin resistance and glucose intolerance with increased WAT.

To clarify whether reduced bone formation and increased adiposity were due to reduced IL-11 expression in the bone or in the adipose tissue, we created conditional IL-11 knockout mice by crossing *osteocalcin* gene promoter-driven (Ocn-Cre) or *adiponectin* gene promoter-driven Cre recombinase transgenic mice (Apn-Cre) with *IL-11* gene floxed (IL-11$^{fl/fl}$) mice (**Supplementary Fig. 8**, Fig. 6a). Osteoblast/osteocyte-specific *IL-11* gene deletion in Ocn-Cre;IL-11$^{fl/fl}$ mice showed reduced bone mass with decreased cortical and cancellous BMD similar to conventional IL-11$^{-/-}$ mice (Fig. 6b, 6c), whereas adipocyte-specific *IL-11*

gene deletion in Apn-Cre;IL-11$^{fl/fl}$ mice showed no difference in cortical or cancellous BMD from those in control IL-11$^{fl/fl}$ mice (Fig. 6b, 6c). Serum IL-11 and osteocalcin levels were reduced in Ocn-Cre;IL-11$^{fl/fl}$ mice but did not change in Apn-Cre;IL-11$^{fl/fl}$ mice (Fig. 6d). Serum TRAP level was similar in all the groups (Fig. 6d). Expression of osteogenic genes, *Ocn, Runx2* and *Osterix* was suppressed, but of *Rankl, Opg* and *Rankl/Opg* ratio as well as osteoclastic genes, *Ctsk* and *TRAP*, was unchanged in Ocn-Cre;IL-11$^{fl/fl}$ mice (Fig. 6e). Expression of those genes was not different from that of control IL-11$^{fl/fl}$ mice in Apn-Cre;IL-11$^{fl/fl}$ mice (Fig. 6e). Furthermore, while mechanical unloading reduced vertebral cancellous BMD in both control IL-11$^{fl/fl}$ and Ocn-Cre;IL-11$^{fl/fl}$ mice (Fig. 6f, **Supplementary Fig. 9**), mechanical reloading increased BMD to a lesser extent in Ocn-Cre;IL-11$^{fl/fl}$ mice compared to that in control IL-11$^{fl/fl}$ mice (Fig. 6f, **Supplementary Fig. 9**). Thus, osteoblast specific IL-11 deletion in Ocn-Cre;IL-11$^{fl/fl}$ mice recapitulated all the bone phenotypes of conventional IL-11$^{-/-}$ mice. Furthermore, AT area under HFD was larger in Ocn-Cre;IL-11$^{fl/fl}$ than in control IL-11$^{fl/fl}$ mice, but was unchanged in Apn-Cre;IL-11$^{fl/fl}$ mice (Fig. 6g, 6h). Thus, the increase in AT mass by systemic deletion of IL-11 was due to a reduction in osteoblast/osteocyte-derived IL-11 but not adipocyte-derived IL-11. Blood glucose was higher after glucose loading by oGTT, and AUC was larger than control IL-11$^{fl/fl}$ mice in Ocn-Cre;IL-11$^{fl/fl}$ but not in Apn-Cre;IL-11$^{fl/fl}$ mice under both RD and HFD (Fig. 6i). Fasting serum insulin as well as HOMA-IR were higher in Ocn-Cre;IL-11$^{fl/fl}$ mice compated with control IL-11$^{fl/fl}$ and Apn-Cre;IL-11$^{fl/fl}$ mice under RD and HFD (Fig. 6j). These results altogether indicate that only Ocn-Cre;IL-11$^{fl/fl}$ but not Apn-Cre;IL-11$^{fl/fl}$ mice develop insulin resistance and glucose intolerance with increased WAT.

Discussion

The present results unexpectedly demonstrate that adipogenic differentiation is enhanced not only in the bone marrow but also in the extra-skeletal adipose tissue in systemic IL-11$^{-/-}$ and Ocn-Cre;IL-11$^{fl/fl}$ mice. To our knowledge, no previous reports with loss of IL-11 signaling such as IL-11Rα$^{-/-}$ or gp130$^{-/-}$ mice demonstrated changes in the adipose tissue [11, 18]. Because canonical Wnt signal suppresses adipogenesis and enhances osteoblastogenesis [8], and because IL-11 deletion in bone enhances the expression of Wnt inhibitors and suppresses Wnt signaling not only in the bone but also in the adipose tissue, these results suggest that IL-11 acts as an upstream modulator in the expression of Wnt inhibitors to cause these changes. However, the present results do not rule out the possibility that other mediators downstream IL-11 also play a role in regulating osteoblastogenesis and bone formation.

In regard to the role of Wnt signal in the adipose tissue, it was reported that Sost$^{-/-}$ mice exhibited a reduction in adipose tissue accumulation with increased insulin sensitivity, along with a dramatic increase in bone volume [19]. In contrast, sclerostin overproduction by adeno-associated virus transfection in the liver of mice resulted in the opposite phenotype with adipocyte hypertrophy. Those results suggested an endocrine function of sclerostin to regulate adipose tissue metabolism [19]. In addition, targeted deletion of TCF7L2, a TCF family key intracellular effector of the Wnt signaling, in adipocytes was shown to promote adipocyte hypertrophy and impaired glucose metabolism [20]. In humans, the

administration of anti-sclerostin antibody, romosozumab, to patients with osteoporosis markedly increased bone formation and bone mass but there has been no report that demonstrated an effect of romosozumab in improving obesity. The present study demonstrated that the expression of other Wnt inhibitors, Dkk1, 2, in the adipose tissue was also upregulated in IL-11$^{-/-}$ mice. Taken together, those previous observations along with the present results are consistent with the notion that Wnt signal downstream IL-11 plays an important role in the negative regulation of adipose tissue mass. Although the present observations do not rule out the possibility that IL-11 may regulate other factor(s) which may also affect adipose tissue and bone metabolism, elucidation of the downstream mediators of IL-11 is out of the scope of this study. Further studies are needed to clarify this issue.

In the absence of IL-11, WAT is increased with increased size and number of adipocytes with reduced expression of lipolytic enzymes. As in human obesity, the resultant increase in adipose tissue mass enhances the expression of inflammatory cytokines in the adipose tissue, and appears to be responsible for the development of insulin resistance and glucose intolerance. Thus, systemic deletion of IL-11 causes not only a reduction in bone formation with increased adiposity in the bone marrow, but also an increase in systemic adiposity leading to obesity and insulin resistance. These features are reminiscent of those in a family with a missense mutation in LRP6, which developed metabolic syndrome and osteoporosis due to impaired canonical Wnt signaling [21].

In the present study, serum IL-11 is reduced and adipose tissue mass is increased not only in systemic IL-11$^{-/-}$ mice but also in Ocn-Cre;IL-11$^{fl/fl}$ mice, indicating that osteoblast/osteocyte-derived IL-11 acts systemically to regulate adipose tissue mass. These results are another example of systemic hormonal action of bone derived cytokines such as fibroblast growth factor 23 (FGF23) [1] and osteocalcin [3]. Thus, exercise stimulates IL-11 expression in the bone via enhanced mechanical loading, which enhances bone formation via, at least in part, the suppression of Wnt inhibitors. At the same time, increased bone-derived IL-11 in response to exercise acts like a hormone via systemic circulation to control adipose tissue mass.

The present observations demonstrate that, in systemic IL-11$^{-/-}$ mice, BMD of weight-bearing bones was reduced by a reduction in bone formation without change in bone resorption. These results establish that the primary action of IL-11 in osteoblastic cells is to enhance bone formation without affecting osteoclastic bone resorption. A previous report demonstrated that systemic IL-11Rα$^{-/-}$ mice exhibited reduced bone remodeling due to suppressed osteoclast differentiation [11]. In those mice, although bone remodeling was low and all the histomorphometric indices of bone formation were reduced, the alteration was regarded as not a cell autonomous change in osteoblasts but was dependent on communications from other cells [11]. Although reasons for the discrepancy between the systemic IL-11$^{-/-}$ and IL-11Rα$^{-/-}$ mice in bone resorptive activity are not clear, there is a possibility that differences in downstream signaling pathways may exist, as IL-11Rα mediates the other signaling pathways than the ones activated by IL-11. In fact, a later report demonstrated, using osteocyte-specific gp130 deletion in Dmp1-Cre;gp130$^{fl/fl}$ mice, that osteocytic gp130 signaling is required for maintaining bone formation and trabecular bone mass [18]. Actions of all IL-6-type cytokines, including IL-11, are mediated through their

common receptor subunit gp130 to potently activate STAT3, and to a lesser extent STAT1 [22]. In the present study, wild-type MC3T3-E1 osteoblastic cells respond to IL-11 by enhanced phosphorylation of STAT3 and to a lesser extent STAT1, while IL-11Rα-deficient MC3T3-E1 cells do not respond to IL-11 in STAT1/3 phosphorylation, and show enhanced expression of *Sost* without change in *Opg* or *Rankl* expression. These results demonstrate that IL-11 signal in osteoblasts is mediated at least in part via IL-11Rα-gp130-STAT1/3 signaling. However, there has been no report that examined the relationship between STAT signal and Wnt inhibitors, and the pathway for the suppression of Wnt inhibitors remains to be clarified.

We previously demonstrated that mechanical unloading suppressed and reloading enhanced *IL-11* gene expression in the hindlimb of mice *in vivo*. The signaling cascade to enhance *IL-11* expression by mechanical loading was examined *in vitro*. Fluid shear stress to mouse primary osteoblasts enhanced Ca^{2+} influx via gadolinium-sensitive cation channel, which activated CREB via phosphorylation of ERK1/2. Activated CREB enhanced *fosB* gene transcription and increased ΔFosB expression [13]. A previous report demonstrated that ΔFosB transgenic mice exhibited enhanced bone formation and increased bone mass [23]. The increased ΔFosB formed complex with JunD on the AP-1 site of *IL-11* gene promoter, and enhanced *IL-11* transcription [4]. Mechanical loading increased IL-11 and suppressed the expression of Wnt inhibitors in osteoblastic cells, while mechanical unloading reduced IL-11 expression and enhanced the expression of Wnt inhibitors [4]. In the present study, the expression of Wnt inhibitors is not suppressed by mechanical loading in IL-$11^{-/-}$ mice, and bone formation in response to mechanical loading is blunted in association with sustained high expression of Wnt inhibitors. These results indicate that IL-11 is a mechano-sensitive cytokine in the bone and plays an important role in regulating bone formation in response to mechanical loading. However, it is still unclear if the stimulation of IL-11 expression in bone is mediated via other mechano-sensors, such as cilia, integrins, G-proteins, Piezo-1 and other calcium channels. In addition, the present study does not rule out the possibility that the effect of IL-11 on bone is mediated by other mechanism(s) than the suppression of Wnt inhibitors. Further details of mechano-sensing mechanism leading to the enhanced expression of IL-11 as well as the downstream signals of IL-11 leading to enhanced bone formation remain to be clarified.

In conclusion, deletion of IL-11 in osteoblasts/osteocytes causes reduced bone mass with suppressed bone formation without change in osteoclast formation or bone resorption. The reduction in bone formation is associated with a reduction in Wnt signaling via upregulation of Wnt inhibitors. IL-11 deletion in osteoblasts/osteocytes also increases systemic adiposity. Because serum IL-11 level was reduced in Ocn-Cre;IL-$11^{fl/fl}$ mice, and because adipose tissue mass was not altered in Apn-Cre;IL-$11^{fl/fl}$ mice, the present study illustrates the physiologically significant role of IL-11 produced by osteoblast/osteocyte in response to mechanical loading in not only osteogenesis but also systemic adiposity and energy metabolism as a hormone. These findings may lead to a novel therapeutic approach to osteoporosis and metabolic syndrome.

Methods

Generation of IL-11 knockout mice

IL-11 conventional knockout (IL-11$^{-/-}$) mice (Accession No. CDB0614K, http://www2.clst.riken.jp/arg/mutant%20mice%20list.html) were generated by using TT2 ES cells [24] (**Supplementary Fig. 10a**). IL-11$^{-/-}$ mice appeared normal with similar fertilizing ability, body length and growth curve compared to their wild-type (WT) littermates (**Supplementary Fig. 6a,6b**). Genomic PCR confirmed that murine *IL-11* gene was present only in WT mice but not in IL-11$^{-/-}$ mice (**Supplementary Fig. 10b**). Female mice were used for all experiments.

All animal experiments were performed according to the guidelines of the Animal Research Committee, the University of Tokushima Graduate School of Health Biosciences and the Institutional Animal Care and Use Committee of RIKEN Kobe Branch.

Breeding conditions

All the mice were housed in standard conditions, 12 hours light/dark cycle in 22-25°C. Most of the analyses in this study were performed in female mice. To determine the effect of high-fat diet (HFD)-induced obesity, mice of each genotype were allocated into two groups with either a regular diet (RD) or a HFD after weaning at 4 weeks with free access to water. Micro CT analysis of adipose tissue areas was performed at 12 and 24 weeks. The time of each measurement is described in the Figure legends.

Compositions of RD (MFG chow, Oriental Yeast Co. Ltd, Japan) and HFD (F2HFHSD diet, Oriental Yeast Co. Ltd, Japan) were as follows:

	Protein	Fat	Carbohydrate	Total calorie
	(% calorie)			(kcal/100g)
RD	25.7	13.6	60.7	357
HFD	17.2	54.5	28.3	481

For HFD, the source of fat was tallow (14 wt%), lard (14 wt%) and soybean oil (2 wt%), the source of carbohydrate was sucrose (20 wt%), cornstarch (14.87 wt%), and the source of protein was casein (25 wt%). Other constituents included cellulose powder (5 wt%), AIN-93 vitamin mixture (1 wt%) and AIN-93G mineral mixture (3.5 wt%).

Generation of TOPGAL;IL-11$^{-/-}$ mice

Wnt indicator TOPGAL mice were obtained from The Jackson Laboratory (Bar Harbor, ME, USA). TOPGAL mice were bred with IL-11$^{-/-}$ and WT mice to generate TOPGAL;IL-11$^{-/-}$ and TOPGAL;WT mice.

Generation of conditional IL-11 knockout mice

To establish IL-11 floxed mice (Accession No. CDB1231K: http://www2.clst.riken.jp/arg/mutant%20mice%20list.html) in which exon 4 of IL-11 gene was flanked by loxP sequences, IL-11-targeted mice carrying a flippase (FLP) recognition target (FRT)-flanked neomycin resistance gene cassette were generated by using TT2 ES cells [24] (**Supplementary Fig. 8a**). Because these homozygous IL-11-targeted female mice were infertile, we obtained embryo from these mice, and deleted neomycin cassette using FLP-FRT recombination by electroporation of FLP mRNA into the embryo. Genomic PCR confirmed that the size of murine *IL-11* gene was larger in floxed mice compared with WT mice (**Supplementary Fig. 8b**). Transgenic mice expressing Cre recombinase under the control of osteocalcin promoter (Ocn-Cre) [25] (courtesy of Prof. Hiroshi Takayanagi and Dr. Kazuo Okamoto, University of Tokyo) and adiponectin promoter (Apn-Cre) [26] (courtesy of Prof. Wataru Ogawa and Dr. Tetsuya Hosooka, Kobe University) were mated with IL-11 floxed (IL-11$^{fl/fl}$) mice to obtain conditional knockout mice. Genomic nested PCR of Ocn-Cre;IL-11$^{fl/fl}$, Apn-Cre;IL-11$^{fl/fl}$ and IL-11$^{fl/fl}$ confirmed that exon 4 of IL-11 gene was deleted in the bone only in Ocn-Cre;IL-11$^{fl/fl}$ mice, and was deleted in the AT only in Apn-Cre;IL-11$^{fl/fl}$ mice (**Fig. 6a)**.

Genotyping

Genomic DNA extracted from mice tails was analyzed by PCR. Genotyping was performed according to the genomic PCR protocol. Briefly, 12.7μl ddH_2O, 2μl 10x buffer, 1.6μl dNTP, 0.8μl 12.5pmol/l forward and reverse primers, 0.1μl Ex Taq DNA polymerase (TaKaRa Bio Inc., Japan) and 3μl DNA sample were used. The PCR program used was as follows: 95°C for 5 minutes, followed by 35 cycles of 95°C for 1 minute, 60°C for 1 minute, 72°C for 1 minute, and the final step of 75°C for 5 minutes.

Different primer sets were used to distinguish WT and conventional IL-11$^{-/-}$ mice: for WT forward (intron 2) 5'-agattggagggacagggaat-3', reverse (intron 4) 5'- atttgggggacacaaaacaa-3', and for IL-11$^{-/-}$ forward (exon 2/intron 2) 5'-agctgcacagatggtaggagattg-3', reverse (within NeoR cassette) 5'-tatgatcggaattcgatagcggcc-3'. The sizes of the PCR product of WT allele was 737 bp, and that of KO was 401 bp.

In order to distinguish IL-11$^{fl/fl}$ from WT and conditional knockout mice, we first amplified *IL-11* gene with the following primers: forward (intron 2) 5'-ttgggcacttgacgaagggg-3', reverse (intron 4) 5'-ggcatcttaagacctaggcctc-3'. To distinguish IL-11$^{fl/fl}$, Ocn-Cre;IL-11$^{fl/fl}$, and Apn-Cre;IL-11$^{fl/fl}$, the following

primer sets were used for nested PCR: forward (exon 3) 5’-atgagcgctgggacattggg-3’, reverse (intron 4) 5’-tcatgggctgcgatttgggg-3’. The sizes of the PCR products of IL-11$^{fl/fl}$ and the conditional KO mice, Ocn-Cre;IL-11$^{fl/fl}$ and Apn-Cre;IL-11$^{fl/fl}$, were 890 bp and 254 bp, respectively.

Establishment of *Il11ra* gene knock-out cell lines by VIKING method

CRSPR/Cas9-mediated *Il11ra* gene editing was conducted following the VIKING method described previously [27]. For genome editing of the mouse *Il11ra* gene locus (Ensemble ID: ENSMUST00000098132.10), annealed oligonucleotides comprising the sequences of *Il11ra* gene (5'-CACCGATTCCACCCGCAGTCCTTG-3', 5'-AAACCAAGGACTGCGGGTGGAATC-3') were cloned into pX330 (Addgene; #42230) as a locus-specific cleaving vector. For the VIKING method, a donor vector pVKG1-Puro (Addgene; #108670) and a donor cleaving vector VKG1-gRNA-pX330 (Addgene; #108671) were prepared as VIKING modules.

MC3T3-E1 cells were suspended in Opti-MEM (11058-021; Life Technologies, USA) and transfected with 15 μg DNA in the VIKING modules and *Il11ra* locus-specific cleaving vector using a Lipofectamine LTX reagent (15338100; Life Technologies) according to the manufacturer’s protocol. Transfected cells were seeded into 100-mm dishes and pre-cultured in MEMa without antibiotics for 24 h. Transduced MC3T3-E1 cells were selected following puromycin treatment (0.1 μg/mL) for 14 days to isolate clonal colonies. For genome sequencing, PCR amplification from genomic DNA of each isolated cell line was conducted using primers “5’-TCGTCGGCAGCGTCAGATGTGTATAAGAGACAGACACACACTGTGGGAAGGAAT-3” and “5’-GTCTCGTGGGCTCGGAGATGTGTATAAGAGACAGGACCGAGACACACTGCAGAC-3” with GoTaq master mix (M7132; Promega, USA) or KOD FX Neo (KFX-201; Toyobo, Japan) according to the manufacturer’s protocol. Each PCR product was directly sequenced using next-generation sequencing (MiSeq; Illumina, USA) **(Supplementary Fig. 1a-1c).**

Immunoblotting of phosphorylated STAT1 and 3

Cells were collected and lysed in lysis buffer (Thermo Fisher Scientific) after stimulation of mIL-11 (R&D systems), electrophoresed on a 10% SDS-PAGE, and blotted onto PVDF membranes (Biorad). After blocking, the membranes were incubated with primary antibodies overnight at 4 °C, and then with HRP-conjugated secondary antibodies for 1h. Protein bands were visualized with a SuperSignal West Pico Chemiluminescent Substrate (Thermo Fisher). The sources for the antibodies were as follows: Rabbit monoclonal antibodies to STAT1, STAT3, p-STAT1, p-STAT3, β-actin and goat anti-rabbit IgG antibody (Cell Signaling)

Tail suspension model

Tail suspension was performed as previously described[4]. Female 8-week-old WT and IL-11$^{-/-}$ mice were used. In brief, tails of the mice were suspended to lift off the hind limbs from ground for two weeks. During the period of tail suspension, mice were able to access food and water freely. After the tail suspension, mice were allowed to move freely in the ground for three weeks (Reloading group) or sacrificed (Tail suspension group) to obtain serum and bone samples.

X-gal staining

β-Galactosidase staining of bone tissues and adipocytes was conducted as previously described[28]. Briefly, tissues were collected and fixed in 2% (v/v) paraformaldehyde and 0.02% (v/v) glutaraldehyde for 1 hour, and bone tissues were decalcified in 15% EDTA for 10 days, and then incubated in 0.1% 4-chloro-5-bromo-3-indolyl β-D-galactosidase (X-Gal solution; Wako, Osaka, Japan) at 37°C overnight. Tissues were washed, then followed by post-fixation with 4% paraformaldehyde at 4°C for 16 hours, and rinsed in an ascending series of ethanol, embedded in paraffin, sectioned and counterstained with eosin.

Immunostaining

Tibias were excised and subsequently fixed in 4% paraformaldehyde at 4°C overnight, then decalcified in 15% EDTA for 15 days. Samples were dehydrated in ethanol, embedded in paraffin blocks, and then cut into 10 μm sections. Before staining, the sections were deparaffinized in xylene, and pretreated in 3% (v/v) hydrogen peroxide/methanol (Wako, Osaka, Japan), followed by blocking using Protein Block-Serum Free (Dako, CA, USA). Then slides were incubated in 1.5% normal goat serum for 30 minutes at room temperature using Vectastain ABC Goat IgG kit (Vector Laboratories Inc., CA, USA). The primary antibody (Goat anti-sclerostin, Goat anti-Dkk1, Goat anti-Dkk2, R&D Systems, Minneapolis, MN, USA; and Goat anti-IL-11, Santa Cruz Biotechnology, Dallas, TX, USA) was 1:100 diluted and incubated at 4°C overnight. Slides were washed and incubated in secondary antibody (Vectastain kit) diluted 1:200 for 30 minutes at room temperature, followed by ABC reagent using Vectastain kit for 30 minutes in accordance to the manufacture's protocol. After washing, slides were developed in a working solution of Imm PACT^{TM} DAB Peroxidase Substrate kit (Vector Laboratories Inc., Burlingame, CA, USA), followed by counterstaining with Weak Methyl Green (Dako, CA, USA).

Real-Time PCR analysis

Total RNA was extracted from femoral bones or adipose tissues and isolated with TRIzol reagent (Invitrogen, CA, USA) according to the manufacture's protocol. Complementary DNA was synthesized using PrimeScript RT Master Mix (Takara Bio Inc., Japan). Then samples were subjected to quantitative real-time PCR analysis using ABI 7300 Real-Time PCR system (Applied biosystems, Foster City, CA) with

SYBR® Green Premix Ex Taq™II kit (Takara, Shiga, Japan). The sequences of primers are listed in **Supplementary Table 1**.

ELISA

To determine the serum bone metabolic parameters, Mouse Osteocalcin EIA Kit (Biomedical Technologies Inc., MA, USA), Mouse TRAP Assay (Immuno diagnostic system Ltd, UK) and Alkaline phosphatase (ALP) test kit (Wako, Osaka, Japan) were used for measuring serum samples in accordance with the manufactures' protocols.

Serum leptin, adiponectin and insulin concentrations were measured with Mouse and Rat Leptin ELISA kit (BioVendor, Brno, Czech Republic), Mouse Adiponection ELISA kit (BioVendor, Brno, Czech Republic) and Ultra Sensitive Mouse Insulin ELISA kit (Morinaga Institute of Biological Science, Inc., Yokohama, Japan), respectively, according to the manufactures' protocols.

Micro-computed tomography (μCT) analysis

Before and during μCT scan, mice were anesthetized by inhalation of isoflurane (Abbott, Tokyo, Japan). Mice were placed on abdominal position in 48 mm wide specimen holder with 96 mm pixel resolution. Hindlimbs were extended to keep the femur and spine into right angle, and then scanned from the proximal end of L1 vertebra to the distal end of L5 to measure vertebral BMD, and whole femoral bones were scanned using LaTheta LCT-200 (Hitachi-Aloka, Tokyo, Japan), as previously described[29]. Calvaria bone samples were extracted and stored. Bone mineral density (mg/cm^3) and adipose tissue area were calculated by LaTheta software.

Bone histomorphometric analysis

Mice were double-labeled with 16mg/kgBW calcein (Sigma, St. Louis, USA) at 6 and 2 days before sacrifice. Lumbar vertebra were removed and fixed in 4% paraformaldehyde (PFA) at 4°C overnight, followed by dehydration with a series of ethanol, then embedded in methyl methacrylate monomer (MMA, Wako, Japan). The plastic sections were cut by a standard microtome (LEICA) into 7 μm samples for von Kossa staining and 4 μm for TRAP and Toluidine blue staining. Histomorphometric analysis was performed by OsteoMeasure (OsteoMetrics, Inc.,GA, USA) according to the ASBMR guideline[30].

Ex vivo cell culture

Bone marrow cells were extracted from 12-week-old female mice. For osteoblastic differentiation, bone marrow stromal cells (BMSC) were cultured in α-Modified Eagle's minimal essential medium (α-MEM; Gibco, NY, USA) supplemented with 10% fetal bovine serum (FBS, Thermo, Utah, USA) and induced with 50μg/ml ascorbic acid (Wako) and 10mM β-glycerophosphate (Sigma-Aldrich, Tokyo, Japan) (osteoblast differentiation medium). For adipogenic differentiation, BMSC were incubated with 10^{-6}M Troglitazone (Sigma-Aldrich, Tokyo, Japan).

Oil-Red O staining

For Oil-Red O staining, BMSC were cultured for 14 days, fixed and rinsed in 60% 2-propanol for 3 times, then stained with Oil-Red O staining solution (Sigma-Aldrich, Tokyo, Japan) for 30 minutes at room temperature. The cells were again washed and rinsed with 60% 2-propanol. The Oil-Red O positive cell number was counted under microscope.

Alkaline phosphatase (ALP) staining and Alizarin Red staining

For ALP staining, cells were cultured in osteoblast differentiation medium for 7 days and fixed in 3.7% formaldehyde for 10 minutes. Then cells were incubated at 37°C with freshly prepared 1mg/ml Naphthol-AS phosphatase (Wako), 6mg/ml Fast-Blue BB (Wako), 0.5% (v/v) N,N-dimetylformaide, 1mM $MgCl_2$, 1M Tris-HCl (pH=8.8) and stained for 5 minutes. Cells were cultured in osteoblast differentiation medium for 15 days for Alizarin Red staining, fixed in 10% formaldehyde for 10 minutes, washed and stained with 0.2% Alizarin Red (Sigma)/1M Tris-HCl (pH=8.3) at 37°C for 20 minutes.

Determination of adipocyte size and number

Visceral fat pad was extracted to determine the adipocyte size and number as previously described [31]. In brief, WAT was fixed with osmium tetroxide (Sigma-Aldrich, Tokyo, Japan) and suspended in isotonic saline. To remove fibrous elements and trap adipocytes, samples were passed through 250μm and 25μm nylon filters, respectively. Adipocyte size was analyzed using a Coulter counter equipped with a 560μm aperture tube and a multichannel particle analyzer (Multisizer II, Coulter Electronics, Fullerton, CA). Adipocyte relative number was determined by dividing the total WAT weight (mg) by the estimated mean adipocyte weight (mg), which was calculated by adipocyte density (0.948mg/ml) × mean adipocyte volume (the average value of adipocyte diameter).

Glucose tolerance test and Insulin tolerance test

Mice were fasted for 16 hours before oGTT and then administrated with 1 g/kgBW glucose orally. Blood samples were collected from mice tails at various time points, and blood glucose was measured by glucometer (Medisafe mini GR-102, Terumo, Tokyo, Japan). HOMA-IR (homeostatic model assessment insulin resistance) as an index of insulin sensitivity was calculated by the following formula, where 100 pg/mL insulin corresponds to 2.6 mU/mL:

Fasting serum insulin (mU/mL) x fasting blood glucose (mg/dL) / 405 = HOMA-IR

Statistical Analysis

Data are presented as mean ± SD. The significance of difference between two groups was assessed by the Student's t-test, and the difference among multiple groups was evaluated using ANOVA test followed by appropriate post-hoc tests as described in the figure legends with SPSS version 21.0 (Chicago, USA). $P < 0.05$ was considered as statistically significant.

References

1. Kinoshita, Y. & Fukumoto, S. X-Linked Hypophosphatemia and FGF23-Related Hypophosphatemic Diseases: Prospect for New Treatment. *Endocr Rev* 39, 274–291 (2018).
2. Takashi, Y. *et al.* Activation of unliganded FGF receptor by extracellular phosphate potentiates proteolytic protection of FGF23 by its O-glycosylation. *Proc Natl Acad Sci USA* 116, 11418–11427 (2019).
3. Wei, J. & Karsenty, G. An overview of the metabolic functions of osteocalcin. *Rev Endocr Metab Disord* 16, 93–98 (2015).
4. Kido, S. *et al.* Mechanical stress induces Interleukin-11 expression to stimulate osteoblast differentiation. *Bone* 45, 1125–1132 (2009).
5. Kawashima, I. *et al.* Molecular cloning of cDNA encoding adipogenesis inhibitory factor and identity with interleukin-11. *FEBS Lett* 283, 199–202 (1991).
6. Jenkins, B.J. *et al.* Pathologic consequences of STAT3 hyperactivation by IL-6 and IL-11 during hematopoiesis and lymphopoiesis. *Blood* 109, 2380–2388 (2007).
7. Johnstone, C.N., Chand, A., Putoczki, T.L. & Ernst, M. Emerging roles for IL-11 signaling in cancer development and progression: Focus on breast cancer. *Cytokine Growth Factor Rev* 26, 489–498 (2015).
8. Bennett, C.N. *et al.* Regulation of osteoblastogenesis and bone mass by Wnt10b. *Proc Natl Acad Sci USA* 102, 3324–3329 (2005).
9. Girasole, G., Passeri, G., Jilka, R.L. & Manolagas, S.C. Interleukin-11: a new cytokine critical for osteoclast development. *J Clin Invest* 93, 1516–1524 (1994).

10. Taguchi, Y. *et al.* Interleukin-6-type cytokines stimulate mesenchymal progenitor differentiation toward the osteoblastic lineage. *Proc Assoc Am Physicians* 110, 559–574 (1998).
11. Sims, N.A. *et al.* Interleukin-11 receptor signaling is required for normal bone remodeling. *J Bone Miner Res* 20, 1093–1102 (2005).
12. Takeuchi, Y. *et al.* Interleukin-11 as a stimulatory factor for bone formation prevents bone loss with advancing age in mice. *J Biol Chem* 277, 49011–49018 (2002).
13. Inoue, D., Kido, S. & Matsumoto, T. Transcriptional Induction of FosB/{Delta}FosB Gene by Mechanical Stress in Osteoblasts. *J Biol Chem* 279, 49795–49803 (2004).
14. Kodama, Y. *et al.* Reduced expression of interleukin-11 in bone marrow stromal cells of senescence-accelerated mice (SAMP6): relationship to osteopenia with enhanced adipogenesis. *J Bone Miner Res* 13, 1370–1377 (1998).
15. Kuriwaka-Kido, R. *et al.* Parathyroid hormone (1–34) counteracts the suppression of interleukin-11 expression by glucocorticoid in murine osteoblasts: a possible mechanism for stimulating osteoblast differentiation against glucocorticoid excess. *Endocrinology* 154, 1156–1167 (2013).
16. Miyamoto, A. *et al.* Medical baseline data collection on bone and muscle change with space flight. *Bone* 22, 79S-82S (1998).
17. Watanabe, Y. *et al.* Intravenous pamidronate prevents femoral bone loss and renal stone formation during 90-day bed rest. *J Bone Miner Res* 19, 1771–1778 (2004).
18. Johnson, R.W. *et al.* The primary function of gp130 signaling in osteoblasts is to maintain bone formation and strength, rather than promote osteoclast formation. *J Bone Miner Res* 29, 1492–1505 (2014).
19. Kim, S.P. *et al.* Sclerostin influences body composition by regulating catabolic and anabolic metabolism in adipocytes. *Proc Natl Acad Sci USA* 114, E11238-E11247 (2017).
20. Geoghegan, G. *et al.* Targeted deletion of Tcf7l2 in adipocytes promotes adipocyte hypertrophy and impaired glucose metabolism. *Mol Metab* 24, 44–63 (2019).
21. Mani, A. *et al.* LRP6 mutation in a family with early coronary disease and metabolic risk factors. *Science* 315, 1278–1282 (2007).
22. Heinrich, P.C. *et al.* Principles of interleukin (IL)-6-type cytokine signalling and its regulation. *Biochem J* 374, 1–20 (2003).
23. Sabatakos, G. *et al.* Overexpression of DeltaFosB transcription factor(s) increases bone formation and inhibits adipogenesis. *Nat Med* 6, 985–990 (2000).
24. Yagi, T. *et al.* A novel ES cell line, TT2, with high germline-differentiating potency. *Anal Biochem* 214, 70–76 (1993).
25. Zhang, M. *et al.* Osteoblast-specific knockout of the insulin-like growth factor (IGF) receptor gene reveals an essential role of IGF signaling in bone matrix mineralization. *J Biol Chem* 277, 44005–44012 (2002).

26. Lee, K.Y. *et al.* Lessons on conditional gene targeting in mouse adipose tissue. *Diabetes* 62, 864–874 (2013).
27. Sawatsubashi, S., Joko, Y., Fukumoto, S., Matsumoto, T. & Sugano, S.S. Development of versatile non-homologous end joining-based knock-in module for genome editing. *Sci Rep* 8, 593 (2018).
28. Tran, K.V. *et al.* The vascular endothelium of the adipose tissue gives rise to both white and brown fat cells. *Cell Metab* 15, 222–229 (2012).
29. Bouxsein, M.L. *et al.* Guidelines for assessment of bone microstructure in rodents using micro-computed tomography. *J Bone Miner Res* 25, 1468–1486 (2010).
30. Dempster, D.W. *et al.* Standardized nomenclature, symbols, and units for bone histomorphometry: a 2012 update of the report of the ASBMR Histomorphometry Nomenclature Committee. *J Bone Miner Res* 28, 2–17 (2013).
31. Lubura, M. *et al.* Non-invasive quantification of white and brown adipose tissues and liver fat content by computed tomography in mice. *PLoS One* 7, e37026 (2012).

Declarations

Acknowledgements

This study was supported in part by Grants-in-Aid for Scientific Research (#20249050, #25293215 and #16H05327 to TM; #17H05104 and #19K22719 to MH; #18K19518 to SS; and #19H03676 to SF) from the Japan Society for the Promotion of Science.

Author contributions

TM, MA and SF designed the study. BD, MH, IE, TN, SK, MA, SF and TM analyzed the data. BD, MH, IE and TM conducted the experiments. IE, YO, TK, YT and MT acquired the data on bone phenotype. RK and SS created and provided cultured cell lines, and acquired data. SS, HK, and GS created and provided IL-11 gene deleted and floxed mice. BD, MH, YT, MT, HS conducted the experiments on adipose tissue phenotype, oxygen consumption and glucose metabolism, and analyzed those data. TN, SK and TM wrote the manuscript. BD and MH contributed equally to this work. BD thoroughly examined systemic IL-11 deleted mice and originally found the increase in adipose tissue mass. MH followed the study, examined conditional IL-11 deleted mice, and found the importance of IL-11 actions in osteoblasts/osteocytes. Therefore, BD is listed first

Additional Information: Competing Interest Statement

The authors have no conflict of interest related to this work.

Figures

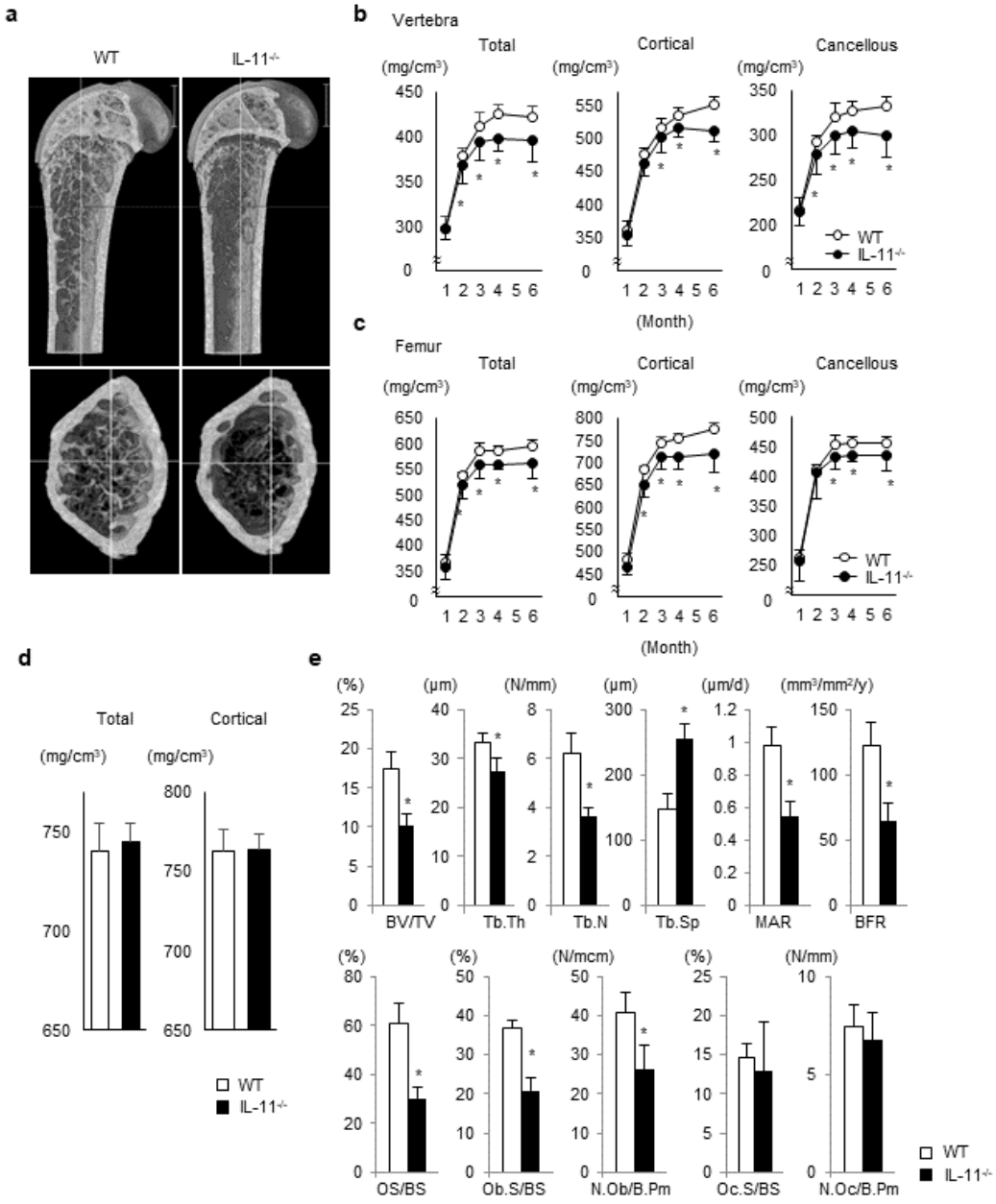

Figure 1

Figure 1

Decreased bone mass with reduced bone formation without change in bone resorption by histomorphometric analysis of the vertebral bone in IL-11-/- mice. (a) Micro-CT of femoral bones from 12-week-old WT and IL-11-/- mice. (b, c) Total, cortical and cancellous bone mineral density (BMD) of

vertebral and femoral bones from WT (open circle) and IL-11-/- mice (closed circle). n=7~9. Data are presented as means ± SD. * P<0.05 compared to WT using two-way repeated measures ANOVA. (d) Total and cortical BMD of calvaria from 12-week-old WT and IL-11-/- mice. n=6~8. Data are presented as means ± SD. (e) Bone histomorphometric analysis of vertebral bones from 12-week-old WT and IL-11-/- mice. BV/TV, bone volume/tissue volume; Tb.Th, trabecular thickness; Tb.N, trabecular number; Tb.Sp, trabecular separation; MAR, mineral apposition rate; BFR, bone formation rate; Oc.S/BS, osteoclast surface/bone surface; N.Oc/B.Pm, number of osteoclasts/bone perimeter; OS/BS, osteoid surface/bone surface; Ob.S/BS, osteoblast surface/bone surface; N.Ob/B.Pm, number of osteoblasts/bone perimeter. n=6. Data are means ± SD. * P<0.05 by Student's t-test.

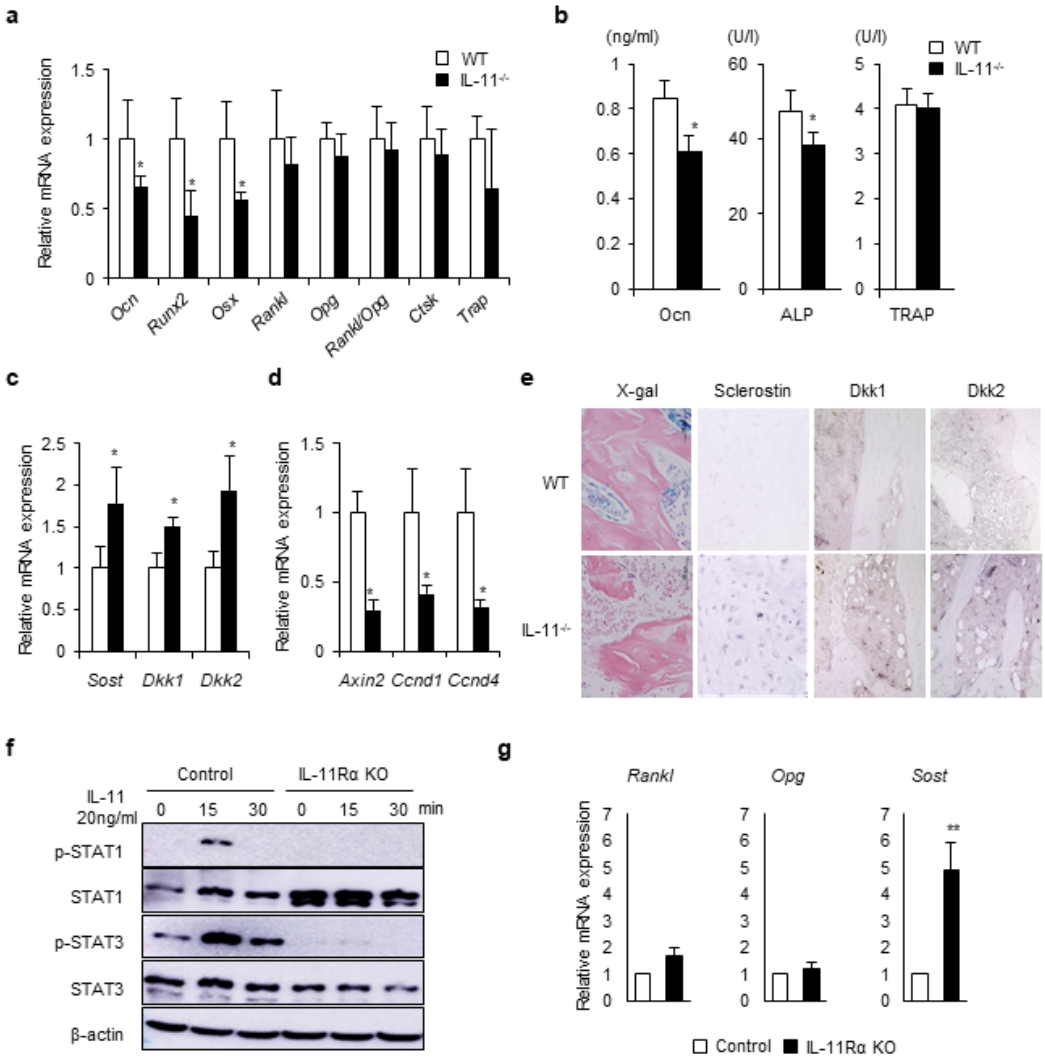

Figure 2

Figure 2

Decreased expression of osteoblastic genes with enhanced expression of Wnt inhibitors and reduced Wnt signaling in the femoral bone, and reduced serum bone formation markers in IL-11-/- mice. (a) Expression of osteoblastic and osteoclastic genes in femur of 12-week-old WT and IL-11-/- mice. n=7~9. Ocn, osteocalcin; Osx, osterix; Rankl, receptor activator of NF-kB ligand; Ctsk, Cathepsin K; Trap, tartrate-resistant acid phosphatase. Data are mean ± SD. * P<0.05 by Student's t-test. (b) Serum bone turnover

markers. OCN, osteocalcin; ALP, alkaline phosphatase; TRAP, tartrate-resistant acid phosphatase. n=5~7. Data are means ± SD. * P<0.05 by Student's t-test. (c) Messenger RNA expression of Wnt inhibitors, and (d) Wnt target genes in femoral bones from 12-week-old WT and IL-11-/- mice. n=7~9. Dkk1, Dickkopf1; Ccnd1, Cyclin D1. Data are means ± SD. * P<0.05 by Student's t-test. (e) X-gal staining and immunostaining of tibia from 10-week-old WT and IL-11-/- mice. (f) STAT1,3 phosphorylation after stimulation with 20 ng/ml IL-11 for 0, 15 and 30 minutes. (g) Expression of Rankl, Osteoprotegerin (Opg) and Sost genes in IL-11Rα knockout and control MC3T3-E1 cells. Data are means ± SD. **P<0/01 vs control by Student's t-test.

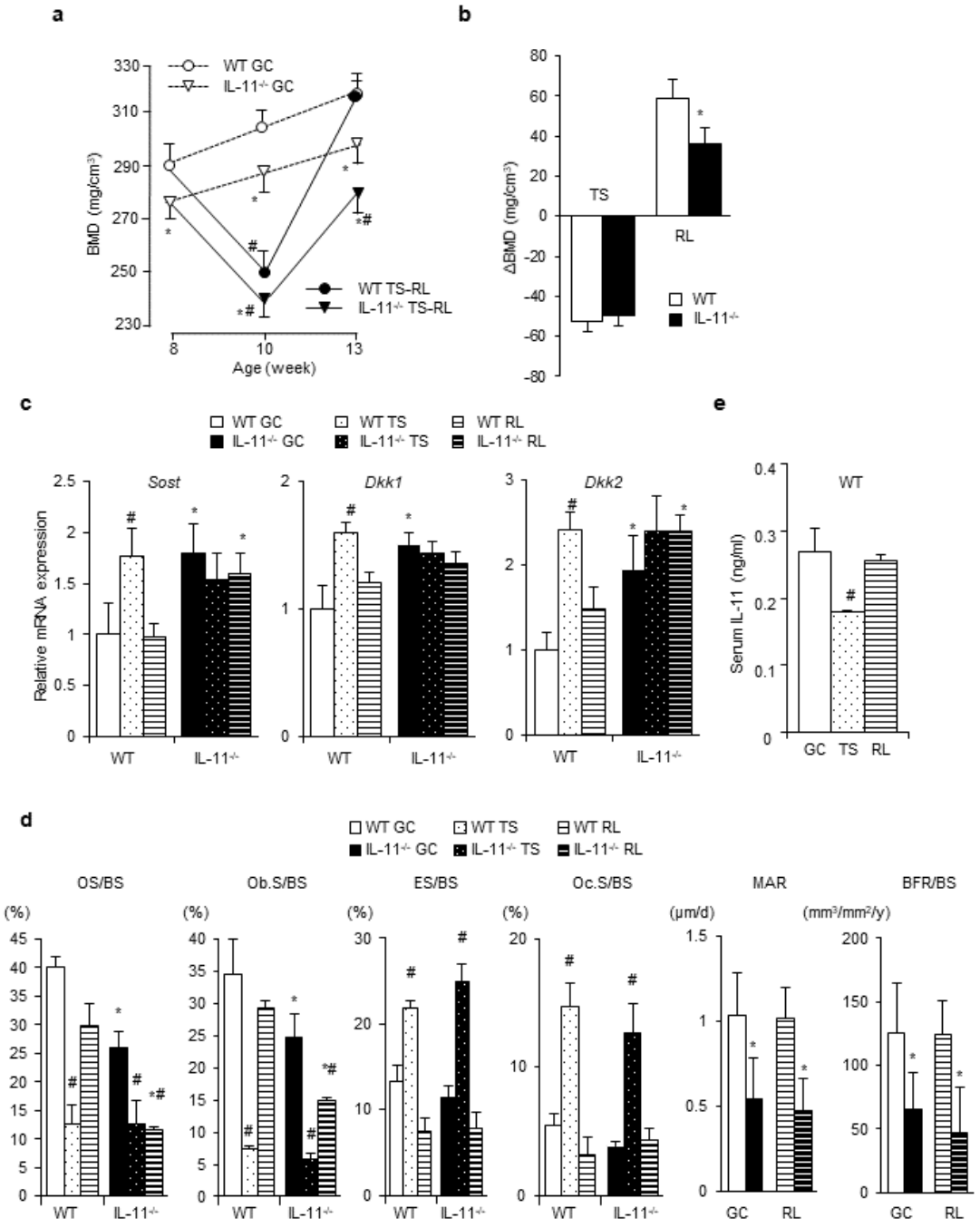

Figure 3

Figure 3

Normal enhancement of bone resorption in response to mechanical unloading, and reduced bone formation in response to mechanical reloading with sustained elevation of Wnt inhibitors in IL-11-/- mice. (a) Vertebral BMD of WT and IL-11-/- mice in ground control (GC), tail suspension (TS) and reloading (RL) groups. n=8~12. Data are means ± SD. *P<0.05 vs WT, #P<0.05 vs GC group in the same genotype using two-way repeated ANOVA with Dunnet post hoc test. (b) BMD change after TS and RL in WT (open bar)

and IL-11-/- mice (closed bar). *P<0.05 vs WT by Student's t-test. (c) Expression of Wnt inhibitors in femoral bones from WT and IL-11-/- mice. n=6~10. Data are means ± SD. *P<0.05 vs WT, #P<0.05 vs GC group in the same genotype using three-way ANOVA with Bonferroni post hoc test. (d) Bone histomorphometric analysis of the vertebrae of WT and IL-11-/- mice. n=3~7. Data are means ± SD. *P<0.05 vs WT, #P<0.05 vs GC group in the same genotype using three-way ANOVA with Bonferroni post hoc test. (e) Serum IL-11 level of WT mice in GC, TS and RL groups. n=6~8. Data are means ± SD. #P<0.05 vs GC group using one-way ANOVA with Bonferroni post hoc test.

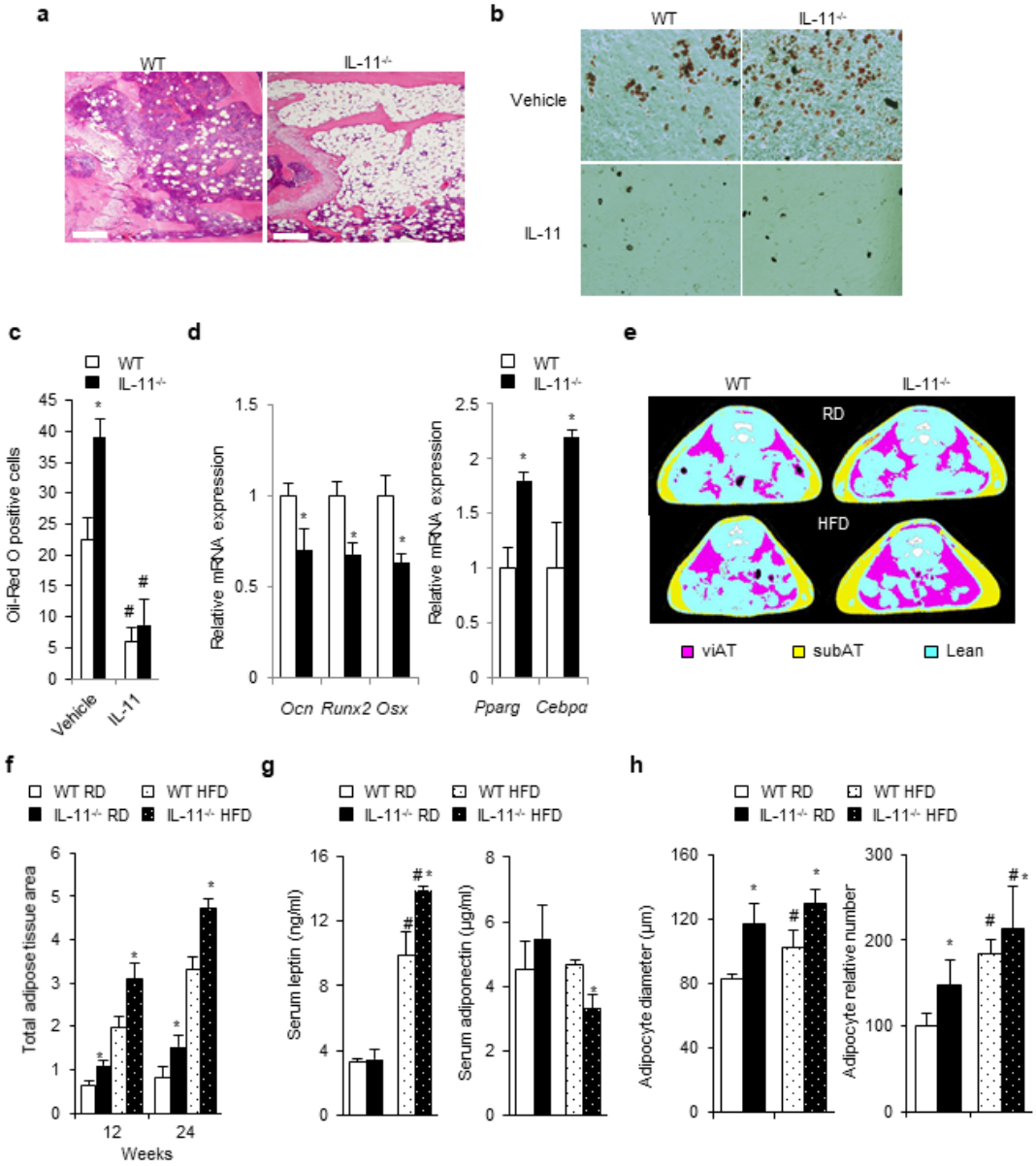

Figure 4

Figure 4

Enhanced systemic adipogenesis along with enhanced adipogenic differentiation with reduced osteogenic differentiation of BMSCs in IL-11-/- mice. (a) H.E. staining of tibia from 16-week-old WT and IL-11-/- mice. Scale bar=1 mm (×100). (b, c) Oil-Red O staining of bone marrow stromal cells (BMSC) from 12-week-old WT and IL-11-/- mice. Adipogenesis was induced by 10-6M troglitazone, with vehicle or 50 ng/ml recombinant IL-11. Data are means ± SD. *P<0.05 vs WT, #P<0.01 vs vehicle group in the same genotypes using two-way ANOVA with Bonferroni post hoc test. (d) Expression of osteogenic and adipogenic genes in BMSC from WT and IL-11-/- mice. Pparγ, peroxisome proliferator-activated receptor γ; Cebpα, CCAAT enhancer binding protein α. Data are means ± SD. *P<0.05 with Student's t-test. (e) Micro-CT analysis at L5 level of WT and IL-11-/- mice on regular (RD) or high-fat diet (HFD) at 24 weeks. Pink, visceral AT (viAT); yellow, subcutaneous AT (subAT); blue, lean mass; white, vertebral bone. (f) Quantitative analysis of total adipose tissue area in WT and IL-11-/- mice on RD or HFD at 12 and 24 weeks. n=9~14. *P<0.05 vs WT on the same diet using two-way ANOVA with Bonferroni post hoc test. (g) Fasting serum leptin and adiponectin in WT and IL-11-/- mice on RD or HFD. n=8. *P<0.05 vs WT on the same diet, #P<0.05 vs RD in the same genotype using two-way ANOVA with Bonferroni post hoc test. (h) Adipocyte diameter and relative number in WAT from 32-week-old WT and IL-11-/- mice on RD or HFD. n=6. Data are means ± SD. *P<0.05 vs WT, #P<0.05 vs RD group in the same genotype using two-way ANOVA with Bonferroni post-hoc test.

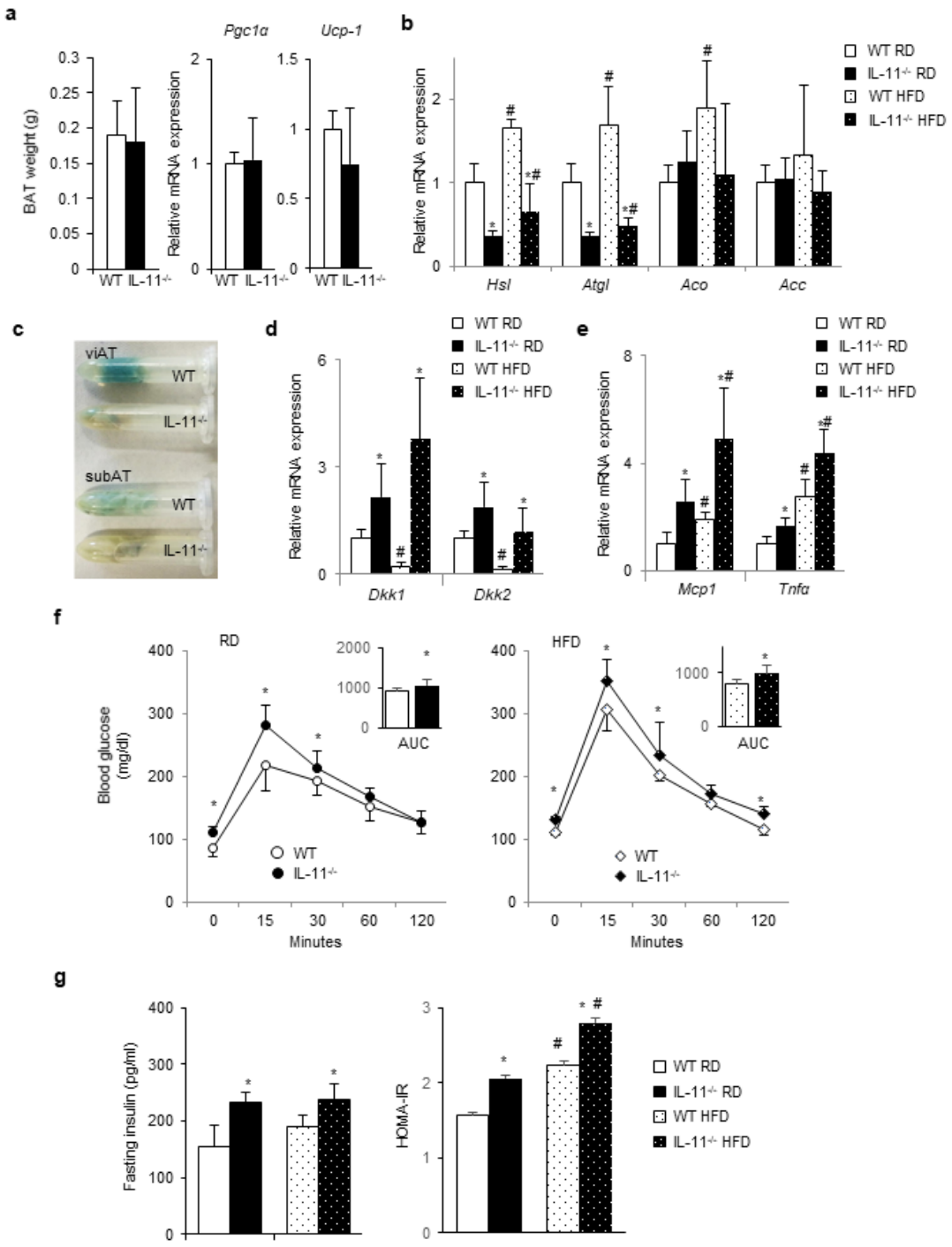

Figure 5

Figure 5

Increased adiposity with reduced expression of lipolytic genes, enhanced expression of inflammatory cytokines, and glucose intolerance with reduced insulin sensitivity in IL-11-/- mice. (a) Brown adipose tissue (BAT) weight and the expression of BAT-specific genes in WT and IL-11-/- mice under RD and HFD. BAT weight and expression of thermogenesis genes, Pgc1α and Ucp-1 in BAT were measured at 12 weeks old. Pgc1α, PPAR-gamma coactivator 1 alpah; Ucp-1, uncoupling protein 1. n= 8. Data are means ± SD.

No significant difference was observed between WT and IL-11-/- mice by Student's t-test. (b) Expression of genes associated with lipolysis (Hsl, hormone-sensitive lipase; Atgl, adipose triglyceride lipase), β-oxidation (Aco, acyl-CoA oxidation,) and lipogenesis (Acc, acetyl CoA carboxylase) in WAT of 32-week-old WT and IL-11-/- mice on RD or HFD. Data are means ± SD. *P<0.05 vs WT, #P<0.05 vs RD in the same genotype using two-way ANOVA with Bonferroni post-hoc test. (c) X-gal staining of visceral (viAT) and subcutaneous AT (subAT) from WT and IL-11-/- mice. (d) Expression of Wnt inhibitors and (e) inflammatory cytokines in WAT from WT and IL-11-/- mice on RD or HFD. n=7~11. MCP1, monocyte chemoattractant protein 1; TNFα, tumor necrosis factor α Data are means ± SD. *P<0.05 vs WT, #P<0.05 vs RD in the same genotype using two-way ANOVA with Bonferroni post-hoc test. (f) Changes in blood glucose by oral glucose tolerance test (oGTT) in 24-week-old WT and IL-11-/- mice on RD or HFD. Insets show AUC of blood glucose. n=6~8. Data are means ± SD. *P<0.05 vs WT by Student's t-test. (g) Insulin levels and HOMA-IR of WT and IL-11-/- mice. n=6. Data are means ± SD. *P<0.05 vs WT, #P<0.05 vs RD in the same genotype by two-way ANOVA with Bonferroni post-hoc test.

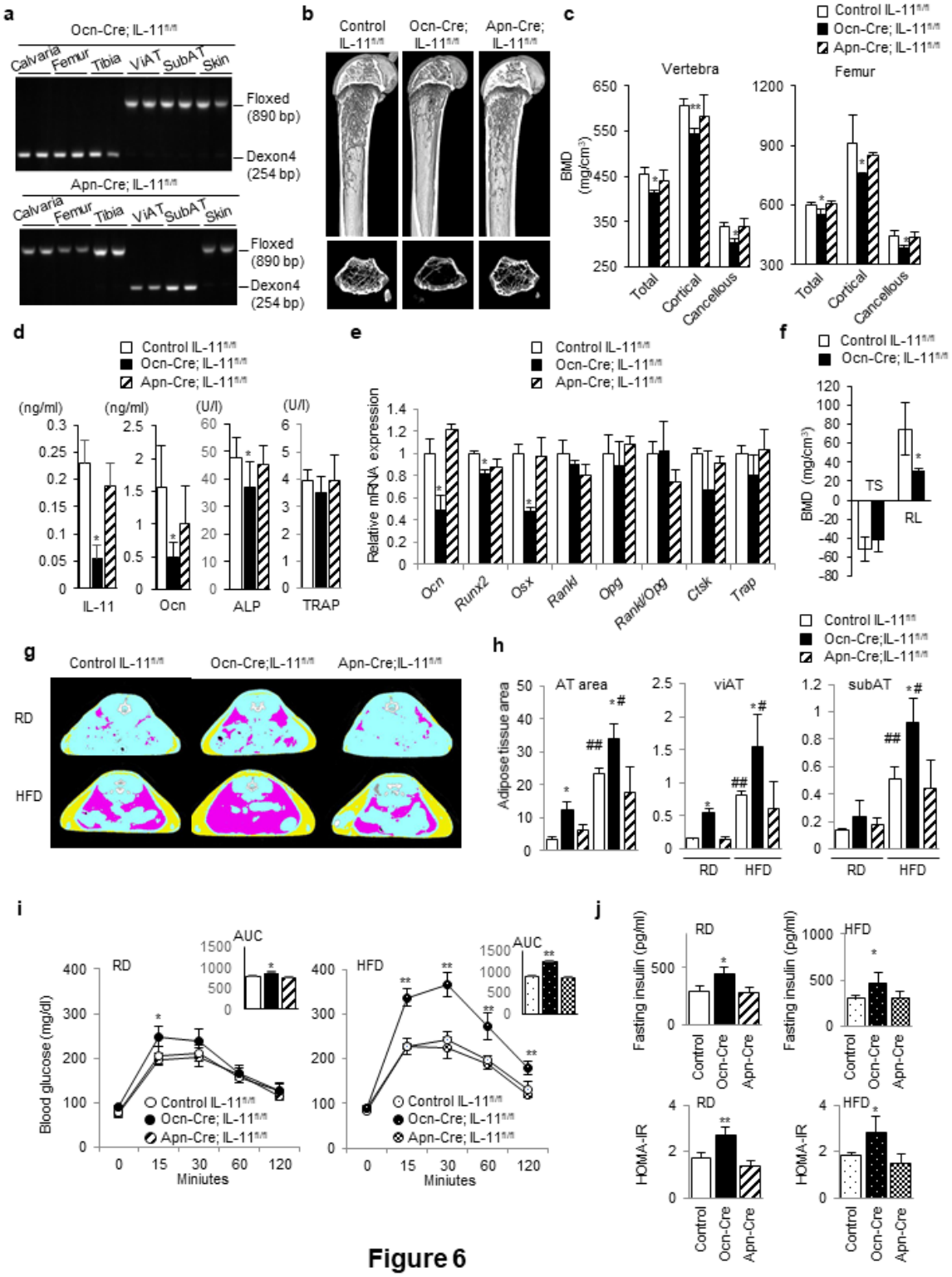

Figure 6

Figure 6

Bone and adipose tissue phenotypes of osteoblast/osteocyte-specific IL-11 deleted mice recapitulate systemic IL-11-/- mice. (a) PCR analysis of genomic DNA extracted from calvaria, femur, tibia viAT, suAT and skin of Ocn-Cre; IL-11fl/fl and Apn-Cre; IL-11fl/fl mice. The sizes of the PCR products from various tissues of IL-11fl/fl and the conditional KO were 890 bp and 254 bp, respectively. (b) Micro-CT of femoral bones from 12-week-old IL-11fl/fl control, osteocalcin (Ocn)-Cre; IL-11fl/fl and adiponectin (Apn)-Cre; IL-

11fl/fl mice. (c) Total, cortical and cancellous BMD of vertebral and femoral bones from 12-week-old IL-11fl/fl control, Ocn-Cre; IL-11fl/fl and Apn-Cre; IL-11fl/fl mice. n=5~6. Data are means ± SD. *P<0.05 and **P<0.01 vs control using one-way ANOVA with Bonferroni post-hoc test. (d) Serum IL-11 and bone turnover markers. n=5~7. Data are means ± SD. *P<0.05 using one-way ANOVA with Bonferroni post-hoc test. (e) Expression of osteoblastic and osteoclastic genes in femurs of 12-week-old IL-11fl/fl control, Ocn-Cre; IL-11fl/fl and Apn-Cre; IL-11fl/fl mice. n=7~9. Data are means ± SD. *P<0.05 vs control using one-way ANOVA with Bonferroni post-hoc test. (f) BMD change after TS and RL in control (open bar) and Ocn-Cre; IL-11fl/fl mice (closed bar). *P<0.05 vs WT by Student's t-test. (g) Micro-CT scan at L5 level and (h) quantitative analysis of adipose tissue in IL-11fl/fl control, Ocn-Cre; IL-11fl/fl and Apn-Cre; IL-11fl/fl mice on RD or HFD. Pink, viAT; yellow, subAT; blue, lean mass; white, vertebral bone. AT area at 12 weeks. n=7~9. Data are means ± SD. *P<0/05 vs control on the same diet, #P<0.05 and ##P<0.01 vs RD in the same genotype by two-way ANOVA with Bonferroni post-hoc test. (i) Changes in blood glucose by oral glucose tolerance test (oGTT) in 24-week-old IL-11fl/fl control, Ocn-Cre; IL-11fl/fl and Apn-Cre; IL-11fl/fl mice on RD or HFD. Insets show AUC of blood glucose. n=5. Data are means ± SD. *P<0.05 and **P<0.01 vs control by Student's t-test. (j) Insulin levels and HOMA-IR of IL-11fl/fl control, Ocn-Cre; IL-11fl/fl and Apn-Cre; IL-11fl/fl mice on RD or HFD. n=5. Data are means ± SD. *P<0.05 and **P<0.01 vs control by two-way ANOVA with Bonferroni post-hoc test.

Supplementary Files

This is a list of supplementary files associated with this preprint. Click to download.

- 210817IL11SupplFigXTable.pdf